Solid Freeform Fabrication 2022: Proceedings of the 33rd Annual International Solid Freeform Fabrication Symposium – An Additive Manufacturing Conference
Reviewed Paper

Studies on thin and thick-walled SS316L overhanging specimens manufactured using powder-fed laser-based directed energy

Alexander P. Belchou ‡§, Ashish Jacob †, Sanjay Joshi †, E.W. Reutzel §, Peter Coutts §
‡ Department of Mechanical Engineering,
† Department of Industrial and Manufacturing Engineering,
§ The Applied Research Laboratory,
The Pennsylvania State University, State College, PA 16801
e-mail: apb6435@psu.edu, akj5512@psu.edu, sbj4@psu.edu, ewr101@arl.psu.edu, pjc26@arl.psu.edu

Abstract

Effective Design for Additive Manufacturing (DfAM) requires accurate knowledge of a machine's capabilities and limitations. One important factor is the machine's ability to deposit unsupported overhanging features. A general method was devised to characterize the ability of a powder-fed Laser-Based Directed Energy Deposition (LB-DED) system to deposit overhanging features with various overhang angles, wall thicknesses, and scan strategies, which was then investigated on a DMG Mori LASERTEC 65 3D Hybrid LB-DED system using 3-axis toolpaths. To assess the accuracy of the manufactured overhang angle, for each specimen the angle of the downward facing surface and upward facing surface were measured and compared to the target overhang angle. It was observed that for the longitudinal scan strategy, overhang accuracy substantially degraded as wall thickness increased. For the transverse and cross hatch patterns there is no observable trend between the achievable overhang angle and the wall thickness. In addition, it was observed that in general increasing the target overhang angle degrades the accuracy of the manufactured overhang angle. The most accurate overhang angles overall were achieved for the longitudinal 1 bead thick specimens. These results will help inform future DfAM and path planning strategies. This research fills a gap in the literature by providing a general method to assess overhang capabilities for LB-DED systems.

Introduction and Literature Review

A study on the ability to accurately produce overhanging geometry is crucial to understand the maximum achievable un-supported angular geometry for a laser based directed energy deposition machine. Such studies ensure credence to the manufacturing capabilities of a machine for complex parts with overhanging geometries. However even with the development of new DED systems there is a need to understand its capabilities to ensure confidence to manufacture complex structures. Nassar et al. attempted to derive a novel method to produce overhanging geometries with a 3-axis deposition strategy. They focused on a voxelized approach for the LENS process where voxels were deposited along an overhanging vector geometry [1]. However, formation of large spherical melts limits the method's abilities to achieve good geometric conformity. Kaji et al. focused on deposition of a dome-like structure and observed a 2% deviation along the diameter in a five-axis deposition mode [2]. They observed that usage of a 5-axis configuration enhanced the abilities to achieve greater overhanging geometries for thin-walled dome-based structures. Wang et al. studied the effect of scanning strategies and z increments on the accuracy of overhanging geometries that existed [3]. They observed two different scanning strategies namely reciprocating and unidirectional. The reciprocating strategy

yielded better results in comparison to the unidirectional deposition strategy employed for the deposition of thin-walled specimens. For the reciprocating strategy it was observed that the height of the deposited bead was uniform, and it conformed to the original dimensions of the part to be manufactured. They investigated multiple overhanging geometries and observed deviations in the overhanging angle ranging from 0.6° to 8.6°. Multiple toolpath strategies exist to deposit overhanging structures. Some of them include a principal component analysis-based approach wherein spatial mapping helps generate toolpaths [4]. CAD/CAM packages such as MasterCam, Siemens NX CAM etc. are useful tools for robust toolpath planning. Ertay et al developed a model on a discretized state space thermal history conjoined with a deposition geometry model for the DED process[5]. This model predicts the thermal history and deposition geometry for 2D and 3D toolpaths.

A plethora of work has already been done on overhanging geometries for laser powder bed fusion technologies. The problem is that the addition of support structures to enable overhanging geometries increases build time and cost of manufacturing. Hence a solution which helps maintain geometric accuracy without supports is vital. The capabilities of support free fabrication have been widely underestimated for metal based additive manufacturing processes. The manufacturability of overhanging holes with and without supports has been studied extensively [6]. Overhangs such as these find their application in hydraulic system applications, such as hydraulic valve blocks etc. The researchers revealed the phenomena, called “sagging effect”, in samples with larger diameters (>=18 mm) and larger thicknesses. There were effects on the cylindricity of the samples with increase in hole diameters and thickness of the parts, though little or no effect was observed in the microstructure of the samples. Di et al. conducted studies on overhanging geometries and came up with mitigation strategies to reduce sinking distance due to non-uniform cooling in the LPBF based test specimens by applying an arc around certain sharp corners of overhanging geometries [7]. They concluded that this modification reduced the sinking distance. Such modifications are essential to better designing of supportless parts using this technology. Other research performs analysis of the quality of slopes for multiple geometries including overhanging geometries, using finite element models [8].An interesting approach to a numerical model for PBF was proposed by Jiang et al. [9]. They found that inhomogeneous distribution of the porosity and the effect of gravity on overhang angles played a role in slight deviations in the simulated results, but these fell within an acceptable range. Some other interesting reasons for poor surface quality in overhanging downplane surfaces were studied for the LPBF technology [10]. They found that a thermal capillary action pulled the molten material away from the intended deposition region towards the down plane region. This resulted in dross formations in multiple samples.

Understanding the effects of various parameters and the maximum overhangs achievable for various processes are crucial for scientists who work on topology optimization. This helps them fine tune their algorithms to achieve a higher success rate for steeper overhang angles. An attempt was made by Lianos et al to derive an AM shape optimization method using buildability restriction from existing literature of the DED process[11]. Multiple researchers who perform structural optimization in topology optimization require such studies for their algorithms

[12,13,14,15]. Therefore, such studies in overhanging geometries are crucial to develop robust DfAM strategies for 3-axis DED depositions.

Research Methodology

In order to assess the limitations of depositing overhanging features an experiment was designed to investigate the effect of wall thickness and scan strategy on overhang manufacturability using DED process. The scan strategies investigated were longitudinal, transverse, and crosshatch, as illustrated in Figure 1. The longitudinal scan strategy involved beads running parallel to the overhanging surface, while the beads ran perpendicular for the transverse scan strategy. The crosshatch scan strategy involved alternating the longitudinal and transverse strategies every other layer. The walls investigated for longitudinal were 1 bead thick, 4 beads thick, and 7 beads thick, whose nominal thicknesses were 2.9 mm, 8.2 mm, 13.4 mm respectively. These are the theoretical thicknesses corresponding to a measured 2.9 mm bead width and 40% bead overlap (an example for a 4-bead wall is shown in figure 11). For transverse and crosshatch, 4 bead and 7 bead equivalent wall thicknesses were investigated. Specimens were deposited with a target overhang angle of 3, 6, 9, 12, 15, and 18 degrees from the vertical. The overhang angle was controlled by varying the distance the scan pattern was offset in between layers. A full factorial experiment was performed for the aforementioned parameters, with two replicates each, yielding a total of 84 specimens.

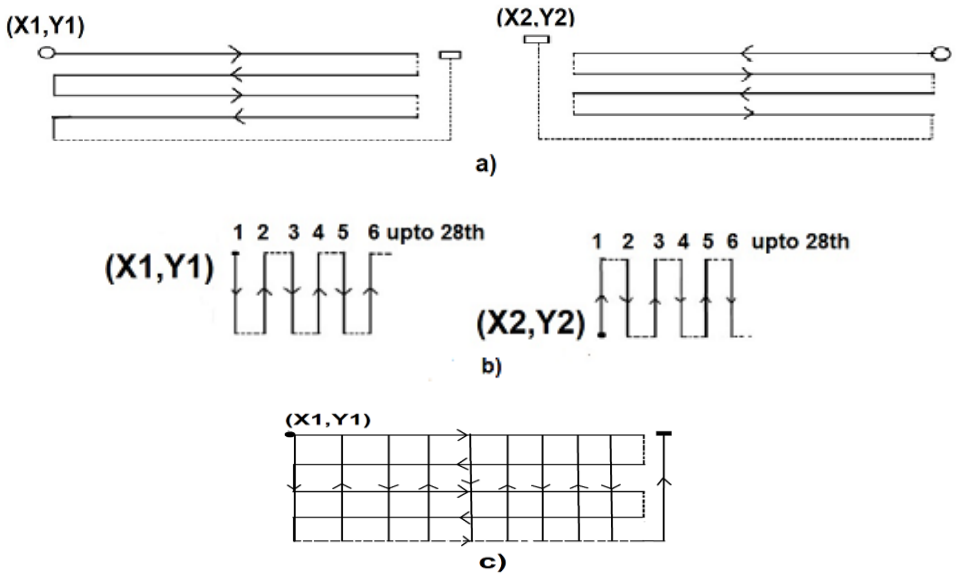

Figure 1. Toolpath example for 4 bead a) longitudinal b) transverse and c) Cross-hatched deposition.

The toolpath for the crosshatch was as follows: 1) longitudinal starting in upper left corner, 2) transverse starting in upper right corner, 3) longitudinal starting in upper right corner, 4) transverse starting in upper left corner. This cycle repeated until all layers had been deposited.

Here (X_1, Y_1) demonstrates the starting point of the first layer and (X_2, Y_2) demonstrates the starting point of the second layer till (X_n,Y_n) where "n" is the total number of layers.

As depicted in Figure 1, the bead direction alternates between both intra and inter layer such that no two adjacent beads have the same direction in all three scan strategies.

Experimentation

The experiments were performed on a DMG Mori LaserTec 65 3D machine using 3-axis planar toolpaths with fixed parameters as shown in Table 1. Corrosion resistant 316L stainless steel substrate 6" x 6"x 1/2" thick was used for each deposition. The powder used was Sandvik SS 316L with grain size in the range 45-150 µm. 8 depositions were made on each substrate. The process parameters used are the typical range for processing SS 316L powder on the DMG Mori Lasertec 65 machine and are listed in Table 1.

Fixed Parameters	Description
Laser Power	1800 W
Laser Spot size	3 mm
Layer thicknesses	0.41 mm (1 bead) 0.67 mm (4 beads) 0.71 mm (7 beads)
Bead width	2.93 mm
Powder feed rate	12 g/min
Traverse speed	1000 mm/min
Bead overlap	40%
Dwell time between layers	15 seconds

Table 1. Processing Parameters used for the experiment.

Before depositing the overhang specimens, a preliminary experiment was performed to determine the bead dimensions, the results of which were incorporated into the G-code for the overhang specimens. A cross section of one of the test beads is depicted in Figure 2.

The nominal dimensions of the overhang specimens were 50 mm long by 21 mm high. The nominal width is 2.9 mm for 1 bead, 8.2 mm for 4 bead, and 13.5 mm for 7 bead. A wedge-like geometry formed in specimens with a higher target overhang angle where the upward facing surface and downward facing surface were not parallel. This is one notable phenomenon where the true width of the specimens differed from the theoretical width.

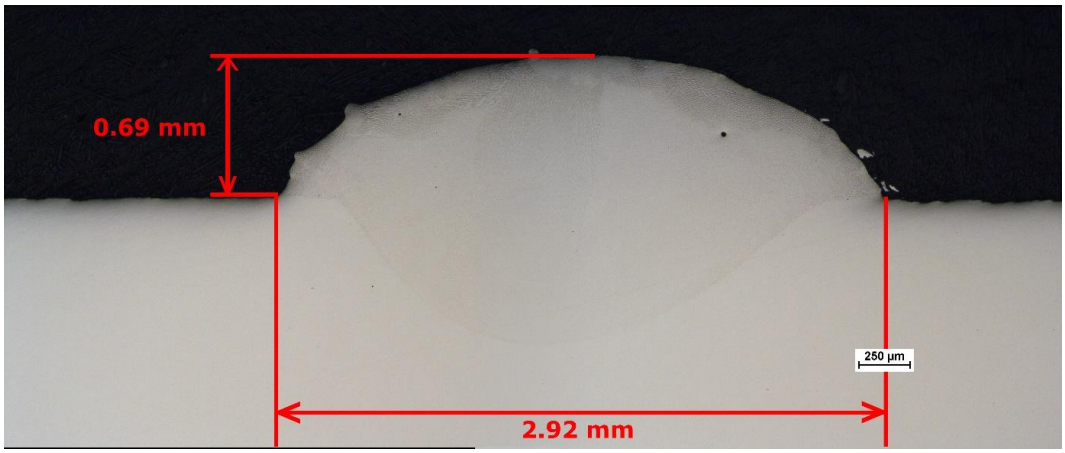

Figure 2. Micrograph depicting one of the test beads.

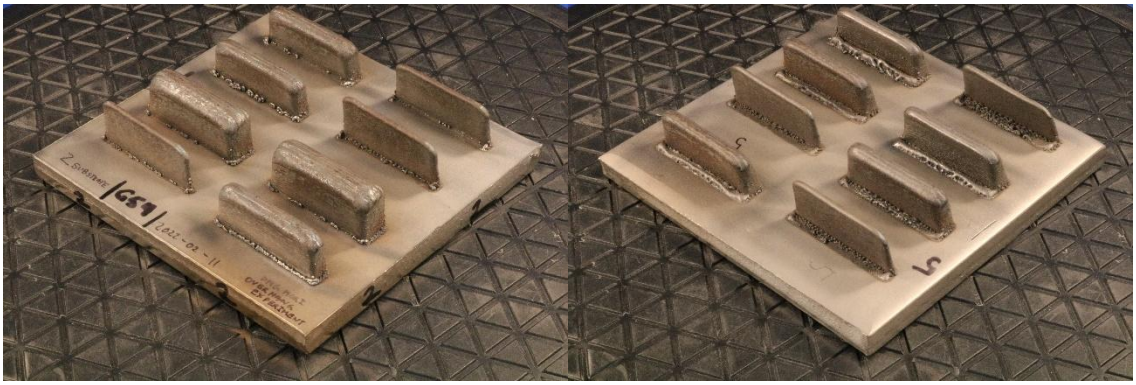

Figure 3. Longitudinal specimens with overhang angles ranging from 3° to 18°.

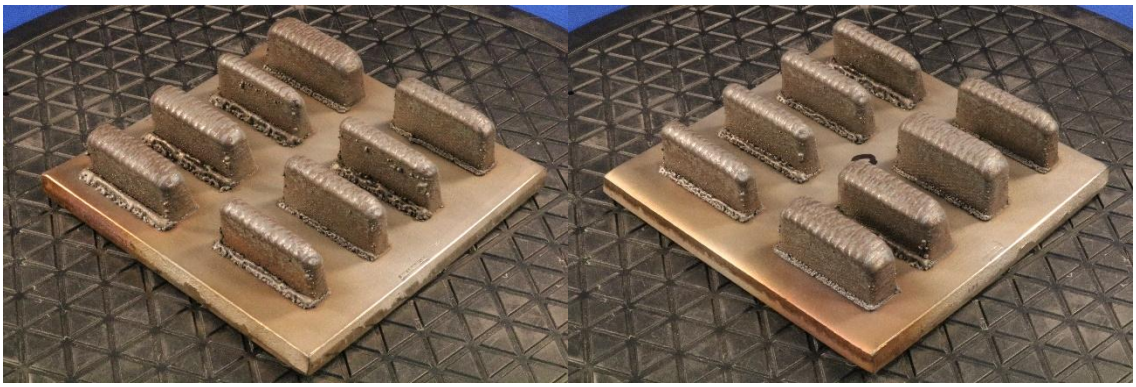

Figure 4. Transverse specimens with overhang angles ranging from 3° to 18°.

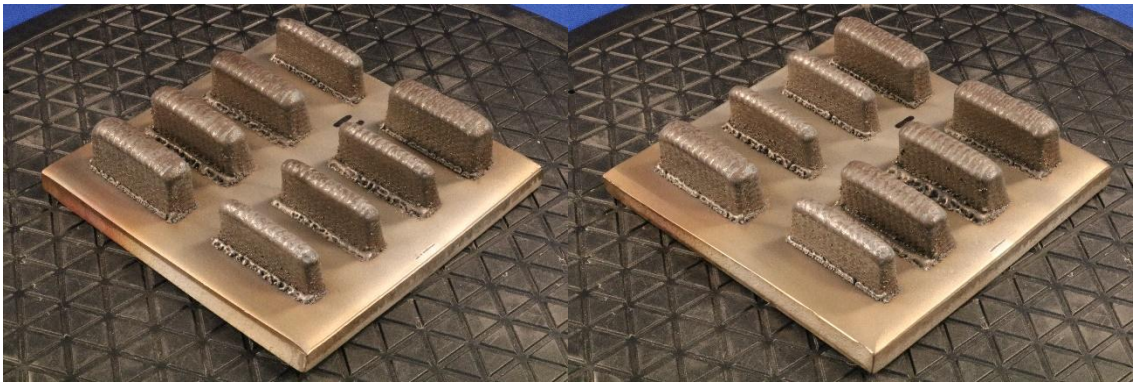

Figure 5. Crosshatch specimens with overhang angles ranging from 3° to 18°.

After deposition, the test specimens and substrates were laser scanned using a FARO Arm Edge. After deposition, the test specimens and substrates were laser scanned using a FARO Arm Edge, a seven-axis arm-based coordinate measuring machine equipped with a laser scanner. Point cloud data was captured and analyzed using Geomagic Control X 3D inspection and metrology software. First, base planes were fit to points at the foot of each specimen on each substrate. These base planes were fit to points occupying a rectangular region of approximately 50 mm by 20 mm. Next, down planes were fit to the downwards facing overhanging surface on each specimen. These down planes were fit to points occupying a rectangular region of approximately 40 mm by 15 mm or roughly 80% of the area of the relevant surface, to capture the global geometry of the surface while avoiding boundary artifacts. Up planes were fit to the upwards facing diagonal surface of each specimen analogously to how the down planes were fit. This is illustrated in Figure 6. For each specimen, the angle was measured between the down plane and the base plane, and the angle was measured between the up plane and the base plane. The overhang down- and up angles were computed as the complements of these aforementioned angles. The overhang down angle is the main parameter of interest since it is the limiting factor in manufacturing overhanging features, while the overhang up angle provides additional insight and a straightforward method of validating the toolpath.

Once the numerical data was extracted for overhang down- and up angles, they were analyzed as follows. Specimens were first grouped by scan strategy (longitudinal, transverse, crosshatch), and then within each scan strategy were subsequently grouped by wall thickness (1 bead equivalent, 4 bead equivalent, 7 bead equivalent). Plots were then made of the overhang angle vs. target overhang angle. The plots were observed to contain trends that are either linear or piecewise linear. The appropriate function (linear or piecewise linear) was fit to each plot, and the fit parameters were used to quantify the overhang manufacturing limitations.

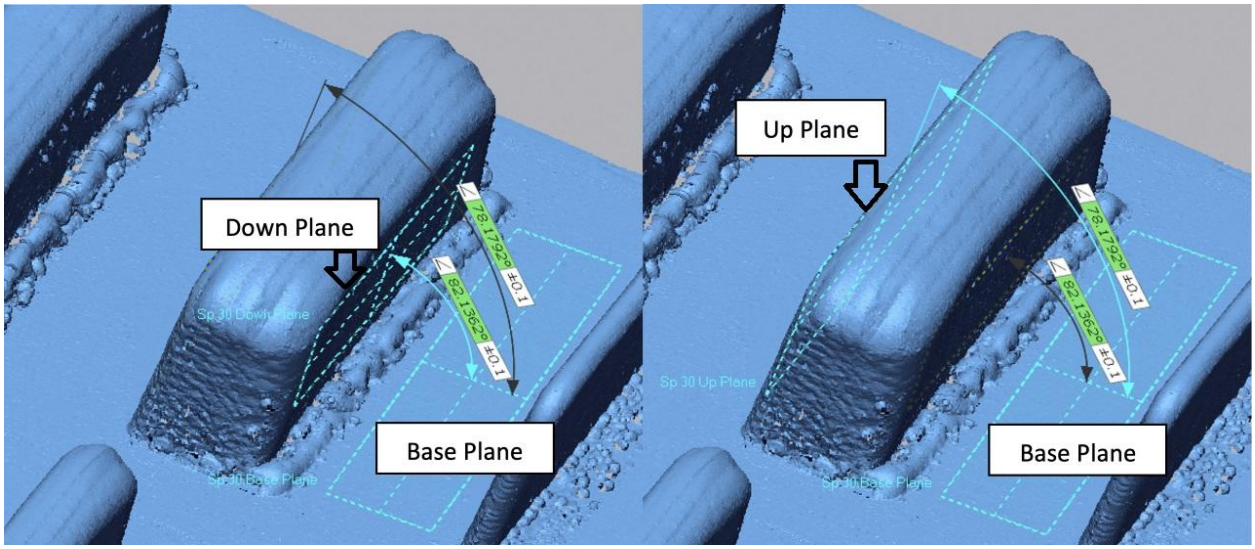

Figure 6. Example depicting base plane, down plane, and up plane for specimen 30 (7 bead wall thickness, 12 degree target overhang).

The plots in Figure 7 summarize the findings of this experiment. The left column contains plots of the angle between the downward facing surface and the vertical, or down-angle. The right column contains plots of the angle between the upward facing surface and the vertical, or up-angle. The down-angle (overhang angle) is the parameter of interest because is limited by the physical dynamics of the deposition. Meanwhile the up-angle serves more as a reference angle since it is mostly determined by the movement of the machine axes. In both columns of plots the identity function is plotted as a dashed line, which represents the ideal deposition trend. For theoretically perfect depositions all points would lie on the dashed line, hence the closeness to said line represents the fidelity of the manufactured angle.

The trends in the up-angles are all linear and are quite close to the identity function, differing by only a few percent. This is to be expected because as previously mentioned, the physical dynamics of manufacturing the upward facing surface is comparatively simple since there is always supporting material below the deposition site.

The plots for the down-angles exhibit more complex trends. The 1 bead longitudinal overhang angles are quite accurate, but the 4 bead and 7 bead have considerable underbuild for the higher angles for all scan strategies. The 4 bead and 7 bead longitudinal initially overshoot the target angle slightly, but severely undershoot after 9 degrees. The 4 bead and 7 bead for both transverse and crosshatch undershoot for all target angles, but the undershoot becomes significantly worse for target angles greater than 12 degrees.

Analysis and Results

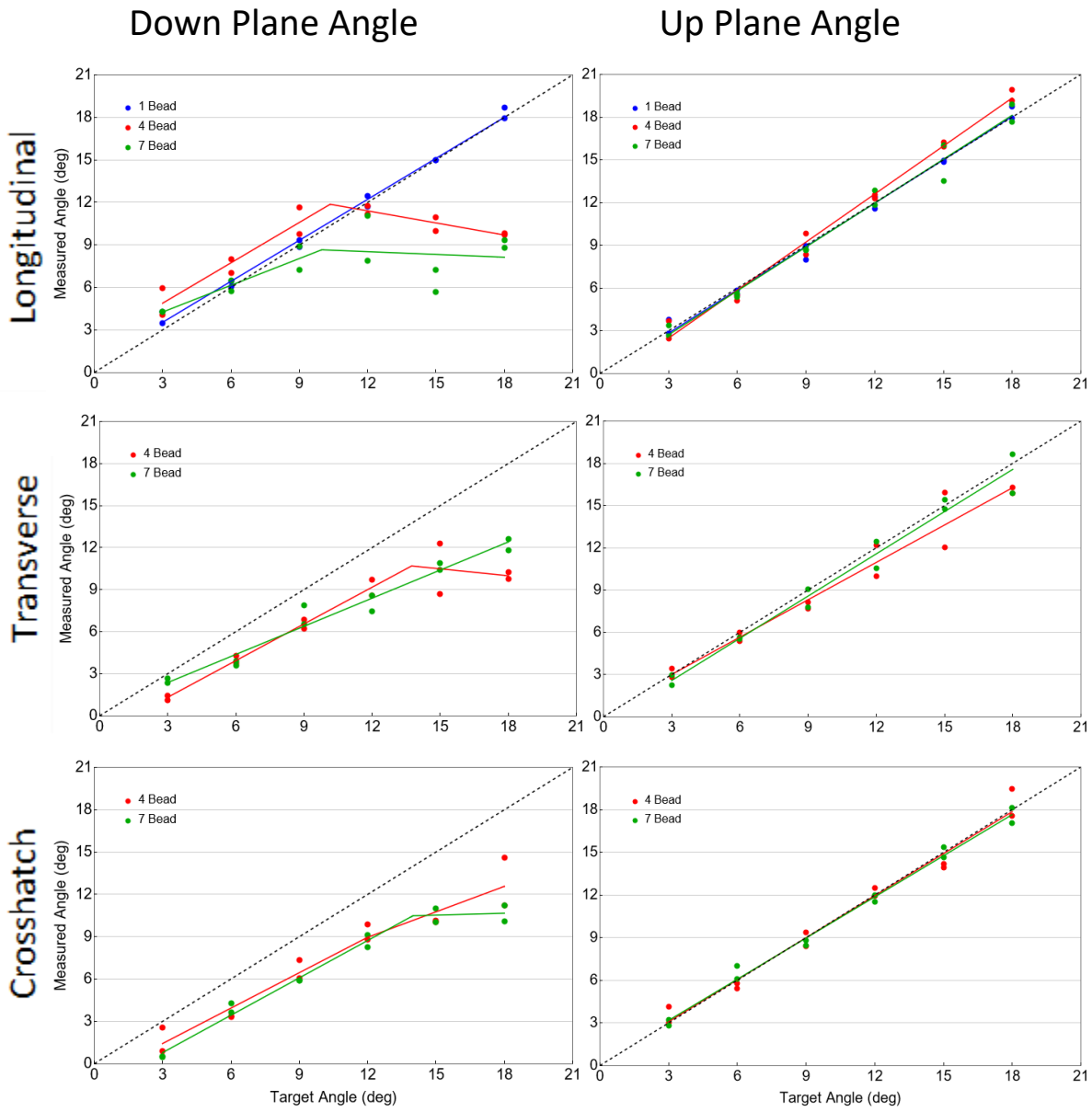

Figure 7. Plots of the measured angle for down- and up-planes as a function of the target angle for the three scan strategies.

As the target angle increases, so does the step over in between layers. This causes a progressively larger fraction of the laser spot and melt pool to be unsupported, which in turn leads to partial failure of the powder to weld to the specimen which results in underbuild. Evidence of this is found in a track of excess material deposited at the foot of each specimen underneath the overhanging surface. As expected, a larger target angle results in this track being larger, as depicted in Figure 8. Figure 9 shows the formation of these excess tracks during deposition. Note that there appear to be three distinct laser spots, while in reality there are two.

The top is the primary laser spot on the specimen and the bottom is the laser spot that has spilled over the edge. What appears to be a middle spot is in fact a reflection.

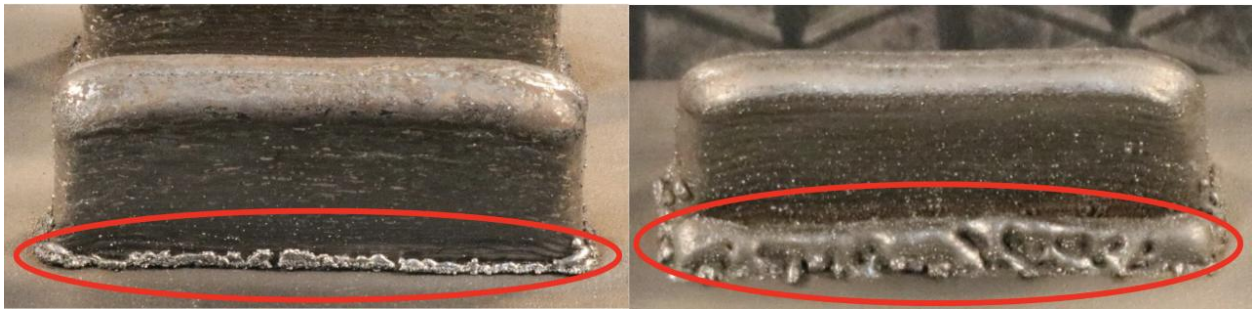

Figure 8. Tracks of material deposited when the laser missed the specimen due to the overhanging toolpath. Depicted for 4 bead 3 degrees (left) and 4 bead 18 degrees (right)

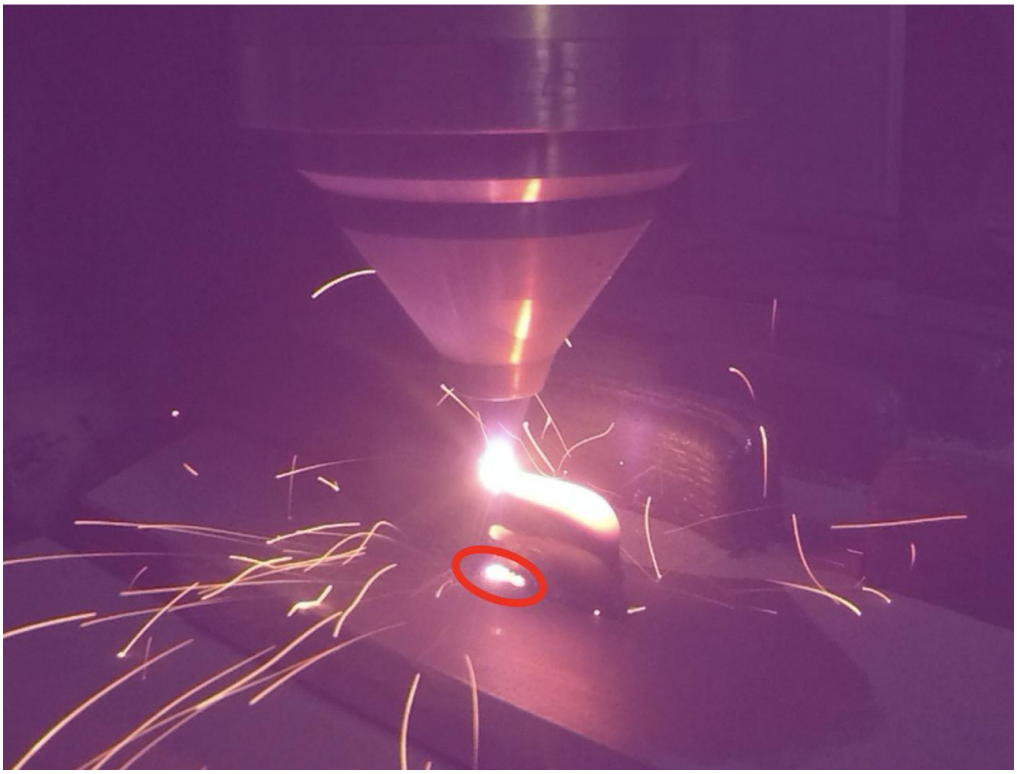

Figure 9. Photograph of deposition showing the formation of the excess tracks.

Summary of overhang findings are depicted in Table 2.

Scan Strategy	Number of beads	Maximum overhang angle(°)	Trend

Longitudinal	1	18.0	Linear with slope of 0.96
Longitudinal	4	11.9	Piecewise (δ=10.4°)
Longitudinal	7	8.7	Piecewise (δ= 10.0°)
Transverse	4	10.7	Piecewise (δ= 13.7°)
Transverse	7	12.4	Linear with slope of 0.67
Crosshatched	4	12.6	Piecewise (δ= 12.0°)
Crosshatched	7	10.5	Piecewise (δ= 14.0°)

Table 2: Summary trends and degradation modes.

Note in the above table δ denotes the point at which the piecewise function changes slope.

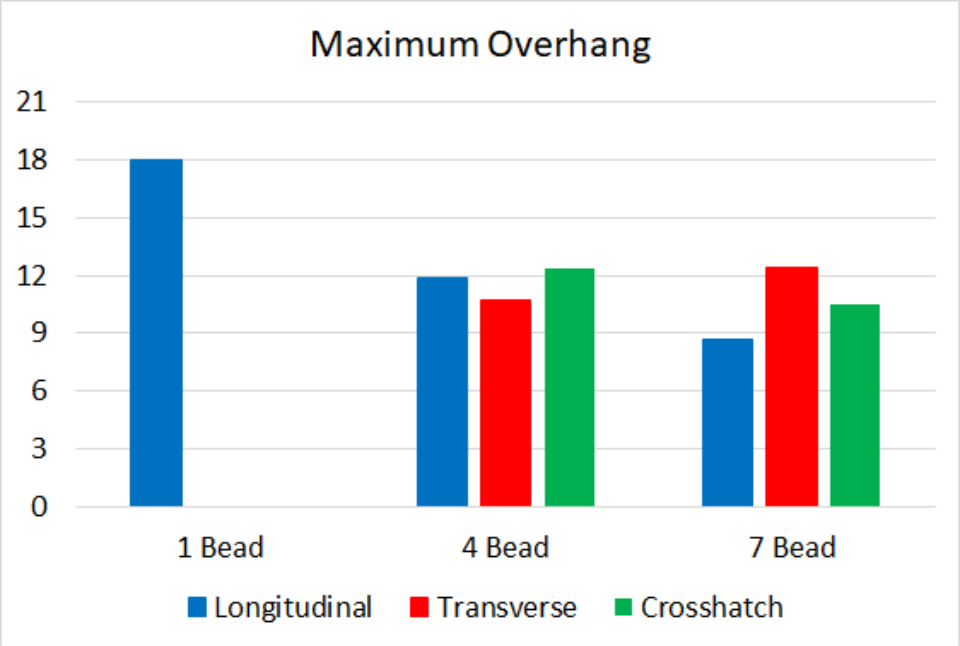

Figure 10. Maximum manufactured overhang for each scan strategy.

Figure 10 shows the maximum overhang angle achieved for each strategy. The longitudinal deposition strategy with 1 bead thickness achieved the maximum overhang angle overall of 18 degrees with a deviation of just 0.7 degrees. The highest deviation for this strategy (and wall thickness) of 1.3 degrees occurred at the target angle of 3 degrees. While the manufactured overhang angles for the 4 and 7 beads were 11.9 and 8.7 degrees respectively. This demonstrates a clear negative trend in the maximum manufacturable overhang angle as the wall thickness increases. As discussed above, the underbuilding is likely due to incomplete support of the laser spot and melt pool.

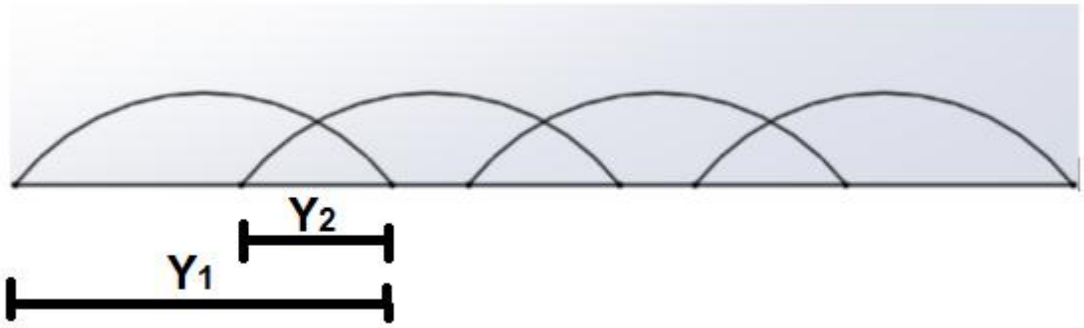

Figure 11. A 4 bead wall with 40% overlapping between each bead ($Y_2 = 0.4Y_1$) where Y_1 represents thickness of a single bead.

For the transverse scan strategy, the 4-bead thickness achieved an overhang angle of 10.7 degrees. This was a slight reduction as compared to the longitudinal scan strategy employed for this wall thickness. The 7-bead thickness showed a slight increase relative to the 4-bead transverse with an overhang angle of 12.4 degrees. By applying this hatch strategy, as the

deposited layers progressed a strong foundation was built due to adequate fusion of the beads. Therefore, the upcoming layers reinforce itself well onto the previous layer. This is the reason why we achieved higher overhang angles for the programmed target angles for the 4 and 7 beads.

The cross hatched deposition strategy showed further improvements (relative to longitudinal and transverse) in the overhang angle with maximum achievable overhang angle being 12.6 degrees for 4 beads, while the 7 beads showed a value of 10.5 degrees situated between longitudinal and transverse. With each deposition the molten material fuses even well with each passing layer. However, the more the thickness more is the time required for the cooling as heat transfer won't happen as quickly as anticipated for a thick specimen, i.e 7 beads in our case. This further affects the depositions, and more and more blobs are seen near the first layer we suspect that the beads tend to stay molten/hot at higher temperatures and the gas flow pushes the material away from the deposition zone. Therefore, thick depositions i.e 7 beads tend to show lower achievable overhang angles.

Conclusion

The following trends were observed regarding the overhang angle as a function of wall thickness and scan strategy.

- First, the 1 bead thick longitudinal specimens demonstrated remarkable capabilities, with the measured overhang angle following the target angle nearly perfectly up to and including 18 degrees. It is very likely that maximum achievable overhang for such a strategy occurs at a significantly higher angle. This high fidelity does not continue for the longitudinal scan strategy as the wall thickness increases. As depicted in Figure 10, there is a clear negative trend in the maximum achievable overhang angle as the wall thickness increases for the longitudinal strategy.
- For transverse and crosshatch strategies, no strong trend was observed between maximum achievable overhang angle and wall thickness. There is a slight positive trend for transverse and a slight negative trend for crosshatch, but it is just a few degrees and likely negligible. In addition, all three scan strategies have approximately the same maximum achievable overhang angle for the 4 bead wall thickness. However, transverse and crosshatch provide a significant benefit over longitudinal for 7 bead wall thickness with transverse coming out on top.
- Another observed trend is that underbuilding of the overhang angle is near universal with the notable exception of the 1 bead thick longitudinal strategy. Therefore, a certain amount of overshoot is necessary in the NC program in order to achieve the desired angle. The necessary amount of overshoot can be determined from the plots in Figure 6.
- Overall, the following conclusions can be drawn: longitudinal with 1 bead thickness provides by far the best accuracy in the overhang angle, all three scan strategies are all but equal for 4 bead thickness, and transverse and crosshatch provide the best performance for 7 bead wall thickness. In addition, underbuild of the overhang angle is common necessitating compensation by programming overbuild of the overhang angle into the NC program.

- Knowing the limitations in manufacturable overhang angle and parameters that affect it allows designers to tune overhanging features in their models to best suit DEDAM. For example, if a large overhang angle is required, a thin wall should be selected. Conversely, if a thick wall is required, overhang angles above 10 degrees should be avoided.

Acknowledgements

This material is based (in part) upon work supported by the CCDC Army Research Laboratory through the Naval Sea Systems Command (NAVSEA) under Contract No. N00024-18-D-6401. Any opinions, findings and conclusions or recommendations expressed in this material are those of the author(s) and do not necessarily reflect the views of the CCDC Army Research Laboratory nor the Naval Sea Systems Command (NAVSEA).

References

[1] Nassar, A. R., and E. W. Reutzel. "Beyond Laser-by-Laser Additive Manufacturing-Voxel-Wise Directed Energy Deposition." In *2014 International Solid Freeform Fabrication Symposium*. University of Texas at Austin, 2015.

[2] Kaji, Farzaneh, Arackal Narayanan Jinoop, Mark Zimny, German Frikel, Kyle Tam, and Ehsan Toyserkani. "Process planning for additive manufacturing of geometries with variable overhang angles using a robotic laser directed energy deposition system." *Additive Manufacturing Letters* 2 (2022): 100035.

[3] Wang, Xinlin, Dewei Deng, Yingbin Hu, Fuda Ning, Hui Wang, Weilong Cong, and Hongchao Zhang. "Overhang structure and accuracy in laser engineered net shaping of Fe-Cr steel." *Optics & Laser Technology* 106 (2018): 357-365.

[4] Dai, Fusheng, Shuaifeng Zhang, Runsheng Li, and Haiou Zhang. "Multiaxis wire and arc additive manufacturing for overhangs based on conical substrates." *Rapid Prototyping Journal* (2021).

[5] Ertay, Deniz Sera, Mihaela Vlasea, and Kaan Erkorkmaz. "Thermomechanical and geometry model for directed energy deposition with 2D/3D toolpaths." *Additive Manufacturing* 35 (2020): 101294.

[6] Ameen, Wadea, Abdulrahman Al-Ahmari, Muneer Khan Mohammed, and Syed Hammad Mian. "Manufacturability of overhanging holes using electron beam melting." *Metals* 8, no. 6 (2018): 397.

[7] Wang, Di, Yongqiang Yang, Manhui Zhang, Jianbin Lu, Ruicheng Liu, and Dongming Xiao. "Study on SLM fabrication of precision metal parts with overhanging structures." In *2013 IEEE International Symposium on Assembly and Manufacturing (ISAM)*, pp. 222-225. IEEE, 2013.

[8] Xiang, Zhaowei, Ling Wang, Chengli Yang, Ming Yin, and Guofu Yin. "Analysis of the quality of slope surface in selective laser melting process by simulation and experiments." *Optik* 176 (2019): 68-77.

[9] Jiang, Dayue, and Fuda Ning. "Anisotropic deformation of 316L stainless steel overhang structures built by material extrusion based additive manufacturing." *Additive Manufacturing* 50 (2022): 102545.

[10] Chen, Hongyu, Dongdong Gu, Jiapeng Xiong, and Mujian Xia. "Improving additive manufacturing processability of hard-to-process overhanging structure by selective laser melting." *Journal of Materials Processing Technology* 250 (2017): 99-108.

[11] Lianos, Andreas K., Harry Bikas, and Panagiotis Stavropoulos. "A Shape Optimization Method for Part Design Derived from the Buildability Restrictions of the Directed Energy Deposition Additive Manufacturing Process." *Designs* 4, no. 3 (2020): 19.

[12] Brackett, David, Ian Ashcroft, and R. Hague. "Topology optimization for additive manufacturing." In *2011 International Solid Freeform Fabrication Symposium*. University of Texas at Austin, 2011.

[13] Langelaar, Matthijs. "An additive manufacturing filter for topology optimization of print-ready designs." *Structural and multidisciplinary optimization* 55, no. 3 (2017): 871-883.

[14] van de Ven, Emiel, Robert Maas, Can Ayas, Matthijs Langelaar, and Fred van Keulen. "Continuous front propagation-based overhang control for topology optimization with additive manufacturing." *Structural and Multidisciplinary Optimization* 57, no. 5 (2018): 2075-2091.

[15] Allaire, Grégoire, Charles Dapogny, Rafael Estevez, Alexis Faure, and George Michailidis. "Structural optimization under overhang constraints imposed by additive manufacturing technologies." *Journal of Computational Physics* 351 (2017): 295-328.

****